ANZIAM J. **63** (2021), 58–69
doi:10.1017/S1446181121000079

EFFICIENT COMPUTATION OF COORDINATE-FREE MODELS OF FLAME FRONTS

B. F. AKERS[✉1] and D. M. AMBROSE[2]

(Received 2 November, 2020; accepted 23 February, 2021; first published online 29 April, 2021)

Abstract

We present an efficient, accurate computational method for a coordinate-free model of flame front propagation of Frankel and Sivashinsky. This model allows for overturned flames fronts, in contrast to weakly nonlinear models such as the Kuramoto–Sivashinsky equation. The numerical procedure adapts the method of Hou, Lowengrub and Shelley, derived for vortex sheets, to this model. The result is a nonstiff, highly accurate solver which can handle fully nonlinear, overturned interfaces, with similar computational expense to methods for weakly nonlinear models. We apply this solver both to simulate overturned flame fronts and to compare the accuracy of Kuramoto–Sivashinsky and coordinate-free models in the appropriate limit.

2020 *Mathematics subject classification*: primary 65M70; secondary 80A22.

Keywords and phrases: flame fronts, coordinate-free models, overturned interfaces..

1. Introduction

We study a model for one-dimensional flame fronts moving in two spatial dimensions, developed by Frankel and Sivashinsky [7]. Such models specify the velocity by which the front moves, in terms of intrinsic geometric information, namely curvature and arclength. While these models allow for general geometries, flame fronts are more commonly studied with weakly nonlinear models such as the Kuramoto–Sivashinsky (KS) equation, which places constraints on the geometry, for instance, that the height of the front is a single-valued function of horizontal position. Recently, Goto et al. directly simulated a model without assuming weak nonlinearity [9]. The numerical method of Goto et al. [9] used finite difference discretization in space and the fourth-order Runge–Kutta method for timestepping, and thus is subject to a classic explicit timestep restriction. In this contribution, we demonstrate that fully nonlinear,

[1]Department of Mathematics and Statistics, Air Force Institute of Technology, WPAFB, OH 45433, USA; e-mail: benjamin.akers@afit.edu.
[2]Department of Mathematics, Drexel University, Philadelphia, PA 19104, USA; e-mail: dma68@drexel.edu.

coordinate-free models may be efficiently simulated. In particular, we introduce a nonstiff method for the initial value problem, which is pseudo-spectral with respect to spatial variables and which uses implicit–explicit (IMEX) timestepping, avoiding the timestep restriction present in [9].

The method is based on the work of Hou, Lowengrub and Shelley (HLS) for interfacial fluid flows with surface tension [10, 11]. The HLS method is based on evolving geometric quantities naturally related to the curvature; specifically, these are the tangent angle the interface forms with the horizontal, and the arclength element. Since curvature and arclength are fundamental to the models of Frankel and Sivashinsky [7], we find that the HLS formulation applies. This formulation, when combined with IMEX timestepping, yields a nonstiff method for the propagation of flame fronts.

Coordinate-free models specify the normal velocity of the flame front; denoting the normal velocity by U and the curvature of the front by κ, one model presented in [7] is

$$-U = 1 + (\alpha - 1)\kappa + \left(1 + \frac{\alpha^2}{2}\right)\kappa^2 + \left(2\alpha + 5\alpha^2 - \frac{\alpha^3}{3}\right)\kappa^3 + \alpha^2(\alpha + 3)\kappa_{ss}. \tag{1.1}$$

With α near unity, and neglecting small terms, another model was derived from (1.1) in [7]:

$$-U = 1 + (\alpha - 1)\kappa + 4\kappa_{ss}. \tag{1.2}$$

The term κ_{ss} is the second derivative of curvature with respect to arclength. The parameter α allows the lower-order term κ to be destabilizing at low wavenumbers/long wavelengths if $\alpha > 1$. For interfaces which are functions of the spatial coordinate, with $\alpha \approx 1$ and small, slowly varying data, these models are approximated by the KS equation

$$y_t + (\alpha - 1)y_{xx} + 4y_{xxxx} + \tfrac{1}{2}(y_x)^2 = 0. \tag{1.3}$$

Frankel and Sivashinsky [7] introduced the coordinate-free models that we study in the case of two spatial dimensions. Other related work includes the extension to three spatial dimensions [8] and the introduction of temperature effects [6]. The numerical simulations conducted in these studies are fully explicit and use finite differences. Of course, fully explicit methods for fourth-order equations have severe stiffness constraints; as mentioned above, we introduce here a pseudo-spectral method using semi-implicit timestepping. Our method is therefore highly accurate without significant timestep constraints. We develop and validate the numerical method in Section 3.

Along with the development of the coordinate-free models in [7], the KS equation is derived as a weakly nonlinear model starting from these coordinate-free models. One may naturally ask, then, as to the validity of the approximations involved in such a derivation. In Section 4, we implement our numerical method to demonstrate the asymptotic validity of the KS equation as an approximation to the coordinate-free models in the appropriate regime. The second author, along with Hadadifard and

https://doi.org/10.1017/S1446181121000079 Published online by Cambridge University Press

Wright, has also demonstrated this validity fully rigorously [3]. A related work is [5], in which solutions of two different weakly nonlinear models related to coordinate-free models of flame fronts are shown to remain close over time; one of these weakly nonlinear models is the KS equation. It is explicitly stated in [5] that the weakly nonlinear models are to be preferred because of the ease of numerical simulation; we demonstrate here that by our method, the full coordinate-free model may be simulated at essentially the same cost.

Another advantage of using the fully nonlinear coordinate-free models which we simulate is that there is no assumption that the interface is a graph with respect to one variable; weakly nonlinear models such as the KS equation inherently have this restriction to graphs. In Section 4, we present an example of a simulated interface with multi-valued height, which is thus beyond the reach of the weakly nonlinear models.

The KS equation has a quite elaborate phase space, including travelling waves, time-periodic waves and chaotic solutions [12]. The chaotic solutions occur for large α or large domain size (or both). In Section 4, we present simulations of the coordinate-free models in the chaotic regime. In one such simulation we observe chaotic trajectories in all three models; in another KS is chaotic, the weakly-nonlinear coordinate-free model evolves to a self-intersecting trajectory, and the fully-nonlinear coordinate-free model has neither chaos nor overturning.

2. Problem formulation

Let a curve $(x(\sigma,t), y(\sigma,t))$ be evolving in $\mathbb{R}^2$; then, we define the arclength element s_σ and the tangent angle the curve forms with the horizontal, θ, as

$$s_\sigma = \sqrt{x_\sigma^2 + y_\sigma^2}, \quad \theta = \tan^{-1}(y_\sigma / x_\sigma).$$

In terms of these quantities, the curvature of the interface is

$$\kappa = \frac{\theta_\sigma}{s_\sigma}. \tag{2.1}$$

We denote a frame of normal and tangent vectors at each point of the curve as

$$\hat{\mathbf{n}} = \frac{(-y_\sigma, x_\sigma)}{s_\sigma}, \quad \hat{\mathbf{t}} = \frac{(x_\sigma, y_\sigma)}{s_\sigma}.$$

We let U denote the normal velocity of the interface and V the tangential velocity:

$$(x,y)_t = U\hat{\mathbf{n}} + V\hat{\mathbf{t}}.$$

In terms of U and V, we may infer evolution equations for s_σ and θ, which are

$$s_{\sigma t} = V_\sigma - \theta_\sigma U, \quad \theta_t = \frac{U_\sigma + V\theta_\sigma}{s_\sigma}. \tag{2.2}$$

https://doi.org/10.1017/S1446181121000079 Published online by Cambridge University Press

We take x and y to be spatially periodic in the following sense:

$$x(\sigma + 2\pi, t) = M + x(\sigma, t), \quad y(\sigma + 2\pi, t) = y(\sigma, t),$$

for a fixed $M > 0$. Then θ is also 2π-periodic: $\theta(\sigma + 2\pi, t) = \theta(\sigma, t)$ for all σ and t.

While U is specified by (1.1) or (1.2), the tangential velocity, V, may be chosen to enforce a preferred parameterization of the front. We take a normalized arclength parameterization. Letting $L(t)$ be the length of one period of the curve, we require s_σ to satisfy $s_\sigma = L/2\pi$. We see then, using the $s_{\sigma t}$ equation in (2.2) together with the requirement that s_σ be independent of σ, that

$$L_t = -\int_0^{2\pi} \theta_\sigma U \, d\sigma. \tag{2.3}$$

With this normalized arclength parameterization, formula (2.1) becomes

$$\kappa = \frac{2\pi\theta_\sigma}{L}. \tag{2.4}$$

We may then write the second derivative of curvature with respect to arclength as

$$\kappa_{ss} = \frac{\kappa_{\sigma\sigma}}{s_\sigma^2} = \frac{\theta_{\sigma\sigma\sigma}}{s_\sigma^3} = \frac{(2\pi)^3\theta_{\sigma\sigma\sigma}}{L^3}. \tag{2.5}$$

We introduce the projection $\mathbb{P}$, which removes the mean of a periodic function:

$$\mathbb{P}f = f - \frac{1}{2\pi}\int_0^{2\pi} f(\sigma)\, d\sigma.$$

The normalized arclength parameterization requires $s_{\sigma t} = L_t/2\pi$, but we also have the equation for $s_{\sigma t}$ in (2.2). This gives us the tangential velocity

$$V = \partial_\sigma^{-1}\mathbb{P}(\theta_\sigma U),$$

where ∂_σ^{-1} is the operator on mean-zero periodic functions which returns an antiderivative with mean zero. In the numerical section that follows, we evolve (2.3) and

$$\theta_t = \frac{2\pi}{L}(U_\sigma + \theta_\sigma \partial_\sigma^{-1}\mathbb{P}(\theta_\sigma U)) \tag{2.6}$$

with U defined as either the fully nonlinear (1.1) or the weakly nonlinear (1.2). In Section 4, we compare the asymptotics of evolution for small-amplitude, slowly varying data with these two models with those for the same data with the KS equation (1.3), essentially testing the effectiveness of KS as an approximate model. We also simulate initial data outside the regime where the models approximate one another for comparison purposes.

3. Numerical method

3.1. Specification of the method In this section we discuss the numerical method and simulations of the coupled system of (2.3) and (2.6) (using either closure (1.1) or

https://doi.org/10.1017/S1446181121000079 Published online by Cambridge University Press

(1.2), coupled with curvature formulas (2.4) and (2.5)). This system is numerically approximated using Fourier collocation for spatial derivatives (as well as for the integral in equation (2.3)). To approximate the time evolution of the discretized system we follow HLS, and implement the fourth-order IMEX scheme of Ascher et al. [4]. This timestepper is designed for an ordinary differential equation of the form $u_t = f(u) + g(u)$ (typically one chooses $f(u)$ to be linear and $g(u)$ as the nonlinearity). It updates as

$$\frac{1}{\Delta t}\left(\frac{25}{12}u^{n+1} - 4u^n + 3u^{n-1} - \frac{4}{3}u^{n-2} + \frac{1}{4}u^{n-3}\right) = f(u^{n+1}) + 4g(u^n) - 6g(u^{n-1}) + 4g(u^{n-2}) - g(u^{n-3}). \tag{3.1}$$

This scheme is not self starting, and one needs to use another scheme for the first three steps. We compare three potential initializations: direct implementation of a fourth-order Runge–Kutta (RK4), an RK4 scheme supplemented with integrating factors (as in [13, 14]), and a third-order Richardson extrapolation of the following first-order IMEX scheme:

$$\frac{u^{n+1} - u^n}{\Delta t} = f(u^{n+1}) + g(u^n). \tag{3.2}$$

All three initializations result in a fourth-order accurate scheme, whose stability restriction is dictated by that of (3.1) in the limit of a small timestep. In practice, the stability restrictions of the initialization manifest when one is far outside their stability region, causing the numerical trajectories to overflow their storage type in the early steps. We present these phenomena in Figures 1 and 2. The linear stability region of RK4 is well known, and we observe that integrating factors do little to ameliorate this stability restriction in this problem. Linear stability analysis on the scheme (3.2), applied to the test problem $f = u_{\sigma\sigma\sigma\sigma}$ and $g = au_\sigma$, gives a scheme which is stable for $\Delta t \leq O(1/a^2)$ (independent of the number of points in space). This is precisely the behaviour we observe numerically when using the Richardson extrapolation of equation (3.2) as an initialization method for (3.1); the resulting scheme's stability properties appear to be independent of spatial resolution.

3.2. Stability of the method As shown in Figure 1, we evaluated the convergence and stability of each initialization method. In the left panel of Figure 1, we fix the number of points in space as $N_\sigma = 16$ and observe that each initialization gives the promised fourth-order accuracy. In the right panel of this figure, we observe that when $N_\sigma = 32$, there is a maximum timestep for which one can use the RK4-based initializations (marked with vertical dashed lines in this panel). The Richardson-extrapolated IMEX1 initialization had no observed timestep restriction when creating these plots. All three methods are ultimately fourth order and stable for a sufficiently small timestep.

In Figure 2, we estimate the Courant–Friedrichs–Lewy (CFL) condition for these schemes by running each scheme at a sampling of N_σ and tracking the largest timestep

https://doi.org/10.1017/S1446181121000079 Published online by Cambridge University Press

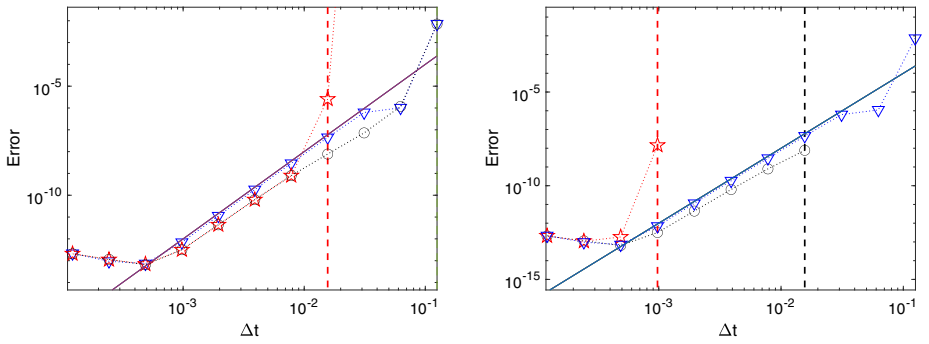

FIGURE 1. Convergence rate of the IMEX4 method (3.1). The markers denote three choices of initialization method. Direct RK4 initialization is marked with stars; RK4 with integrating factors is marked with circles; Richardson-extrapolated IMEX1 is marked with triangles. A solid line at fourth-order accuracy is also shown for comparison purposes. The left panel has $N_\sigma = 16$ spatial points; the right panel has $N_\sigma = 32$ spatial points. The stiffness of this system manifests as a maximum timestep (marked with dashed vertical lines), at which the schemes with RK4 initialization give finite output (the schemes give infinite output to the right of this dashed line). We did not observe any timestep restriction for the Richardson-extrapolated IMEX1 initialization.

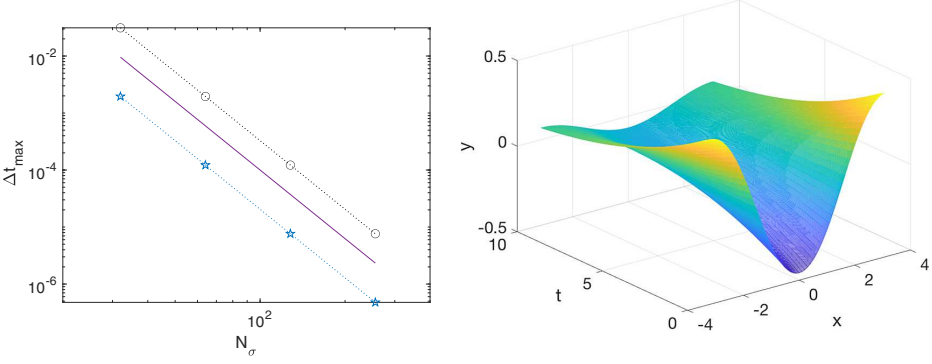

FIGURE 2. Stability of the different initializations of the IMEX4 method. The left panel shows the observed timestep restriction as a function of total spatial points (N_σ) As in Figure 1, the stars correspond to direct RK4 initialization and the circles are the integrating factor RK4 initialization. We did not observe any timestep restriction when initializing with the Richardson-extrapolated IMEX1 scheme (thus, there are no triangles marking its maximum timestep in the left panel). We ran simulations with number of spatial points, N_σ, of up to $2^{16} = 65536$ and observed stable computations with $\Delta t = 0.1$ with this initialization over long times; this simulation is shown in the right panel. The same initial data were used for the simulations shown in the left panel, but with $t < 1/4$.

for which the scheme is stable. For the purposes of this simulation, we call the scheme unstable if it has a solution with $\|\theta\|_\infty > 10$ before $t = 1/4$; the resolved solution we tested on had $\|\theta\|_\infty < \pi/2$. We observe that both RK4-based initializations have a CFL condition which scales like $\Delta t \leq C(\Delta\sigma)^4$ (the solid line in the left panel). The Richardson-extrapolated IMEX1 initialization had no observable timestep restriction;

https://doi.org/10.1017/S1446181121000079 Published online by Cambridge University Press

successful simulations were conducted with the scheme with $N_\sigma = 2^{16} = 65536$ and $\Delta t = 0.1$; see the right panel of Figure 2.

4. Results

4.1. Asymptotic comparison of the models As an application of the numerical method, we compare the evolution of initial data

$$y(x) = \epsilon \sin(\sqrt{\epsilon} x), \quad \alpha = 1 + \epsilon, \tag{4.1}$$

with the KS equation, as well as with the coordinate-free models of Frankel and Sivashinsky which use the normal velocities given in (1.1) and (1.2). To initialize the coordinate-free models, we construct the tangent angle and curve length using

$$\theta = \tan^{-1}(y_x), \quad L = \int \sqrt{1 + y_x^2}\, dx.$$

As the weakly nonlinear coordinate-free model, using (1.2), and the KS equation are approximations of the fully nonlinear coordinate-free model, using (1.1), we consider the fully nonlinear model as the truth and compare the other two models against it. The differences in the evolutions of the initial data (4.1) for the three model equations appear in Figure 3, in which the weakly nonlinear models are denoted as y_M and the fully nonlinear model is denoted as y_F.

The derivation of the KS equation from coordinate-free models in [7] considers data scaled as in (4.1) and keeps terms of size $O(\epsilon^3)$ or smaller. The natural expectation would be for the errors created in this approximation to be asymptotically small compared with $O(\epsilon^3)$ for an $O(1)$ time interval. We observe the infinity-norm-based error for a fixed time interval, which scales as $O(\epsilon^4)$. The asymptotics of the infinity norm and the two-norm of the difference $y_F - y_M$ at both fixed and asymptotically long times are reported in the four panels of Figure 3. These rates match those in [3], suggesting that their rigorous bound has an exponent which is sharp.

4.2. Evolution of an overturned interface The coordinate-free solver discussed here has the same asymptotic cost as the KS equation (all of the equations can be evolved in $O(N_\sigma \log N_\sigma)$ flops per timestep, owing to the Fourier collocation-based spatial discretization). The coordinate-free models have the advantage of being able to evolve initial data for which the interface displacement is not a function of the horizontal coordinate but rather a general parameterized curve. In Figure 4 we present such simulations. For the simulations in Figure 4 we use initial data

$$\theta(\sigma) = A \sin(\sigma), \quad \alpha = 0.1. \tag{4.2}$$

For fixed θ, the curve length, L, and spatial period, M, are related as

$$M = L\left(\frac{1}{2\pi}\int_0^{2\pi} \cos(\theta)\, d\sigma\right)$$

https://doi.org/10.1017/S1446181121000079 Published online by Cambridge University Press

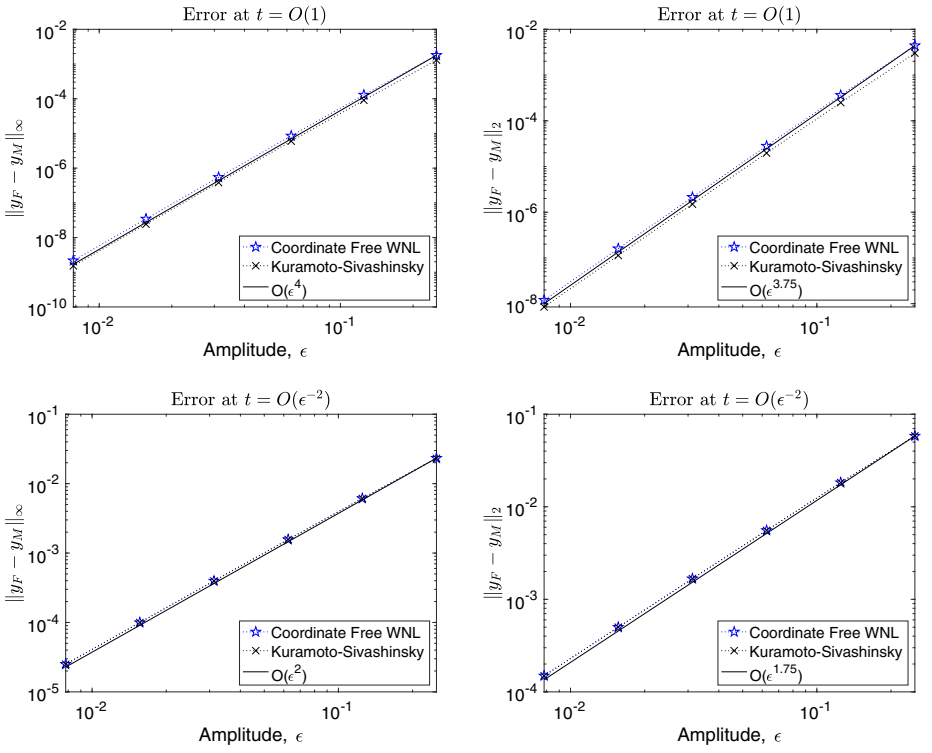

FIGURE 3. Differences in the evolutions of the approximate models, KS (1.3) and the coordinate-free system with weakly nonlinear closure (1.2), and the full coordinate-free model, where the normal velocity closure is (1.1) with initial data (4.1). The top row compares solutions at fixed time; in the bottom row the time is scaled as $O(\epsilon^{-2})$.

or

$$L = M\left(\frac{1}{2\pi}\int \cos(\theta)\, d\sigma\right)^{-1}.$$

We chose to initialize the spatial period, using the latter formula to initialize L.

That the coordinate-free formulation allows for evolution of overturned interfaces means there is a larger simulation space, including allowing for the evolution of self-intersecting interfaces. Self-intersecting interfaces are non-physical, but they do not create a singularity in the parametrically described equation (unlike in some other coordinate-free models such as vortex sheets [1, 2]). An example of the evolution of a multiply self-intersecting interface is shown in the right panel of Figure 4.

4.3. Chaotic solutions It is well known that for large domains (or large α) the KS equation exhibits chaotic trajectories [15, 16]. These chaotic trajectories arise from a range of unstable wavenumbers in the linearization of the KS equation about $y = 0$, which cause small solutions to first become large and then evolve chaotically. The

https://doi.org/10.1017/S1446181121000079 Published online by Cambridge University Press

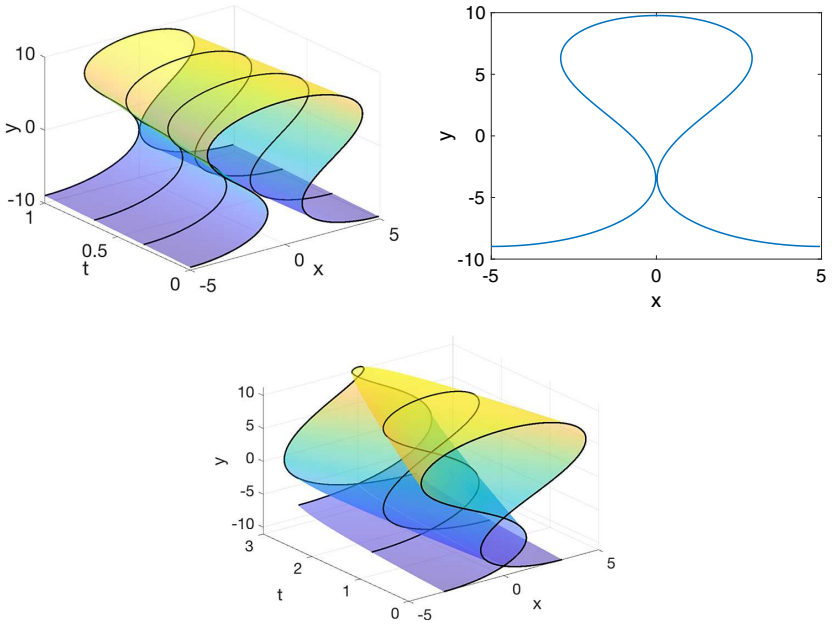

FIGURE 4. The evolution of overturned initial data (4.2) with $A = -11/17\pi$, $L \approx 48.7$, $M = 10$ is shown in the left (time evolution) and centre panels (profile near intersection at $t = 2$). The evolution of an example of self-intersecting initial data, with $A = -7\pi/10$, $L \approx 56.6$, $M = 2\pi$, is shown in the right panel.

phase space of KS is quite elaborate (including travelling waves, periodic solutions and chaos [12]); we do not seek to classify the phase space of coordinate-free models presented here. However, two examples of the chaotic regime are included.

As a first example of a simulation in the chaotic regime, we choose $\alpha = 1.3$ and $L = 250$. This value of α is not so far from one, and the initial data for this simulation are small and slowly varying:

$$y(x, 0) = 0.1 \cos\left(\frac{2\pi}{250}x\right) + 0.1 \cos\left(\frac{4\pi}{250}x\right);$$

thus, one should expect reasonable agreement among the three models. In this simulation, all three models (KS, weakly nonlinear coordinate-free and fully nonlinear coordinate-free) exhibit chaotic trajectories. This regime is depicted in Figure 5. The long-time, chaotic solutions are no longer small, nor do they satisfy the scaling required for the asymptotic equivalence of KS to the fully nonlinear problem. That they are even qualitatively similar could be seen as a victory for KS as an approximate model.

As a second example, we chose $\alpha = 9$, $L = 50$, far from the regime where KS approximates the fully nonlinear problem. Here, the KS equation is still chaotic. The weakly nonlinear coordinate-free model exhibits overturning, which leads to pinch-off in finite time. The solution to the full model has neither chaos nor pinch-off but

https://doi.org/10.1017/S1446181121000079 Published online by Cambridge University Press

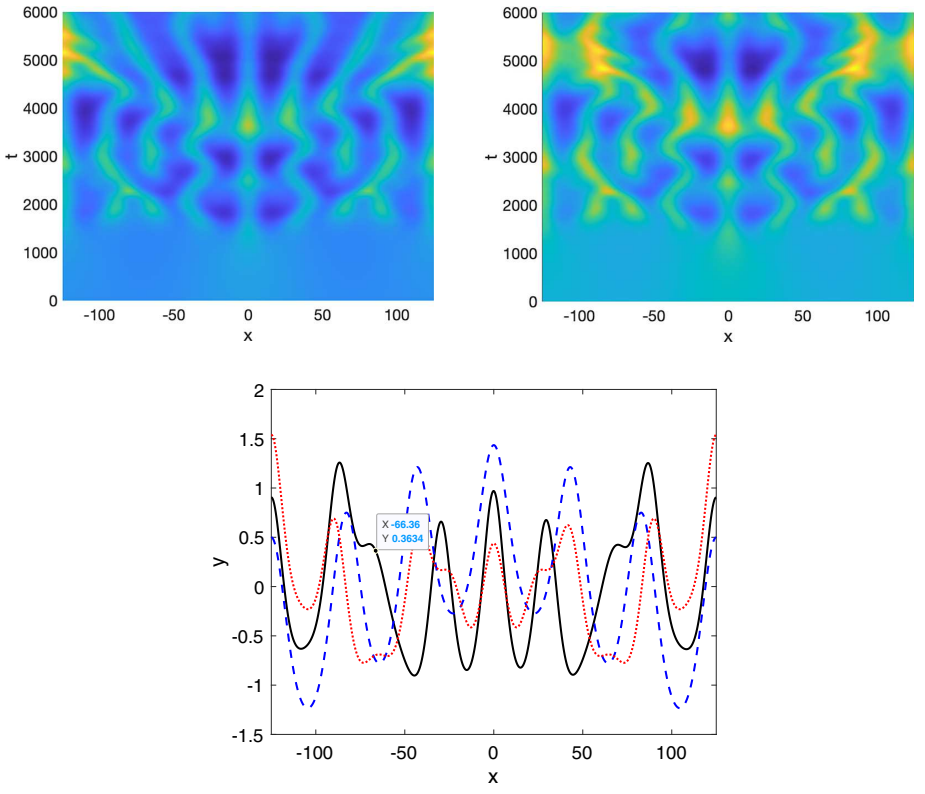

FIGURE 5. Top left: a chaotic trajectory of the KS equation with $L = 250, \alpha = 1.3$, depicted in space time. Top right: a chaotic solution of the fully nonlinear coordinate-free model with $L = 250, \alpha = 1.3$, depicted in space time. Bottom: the solutions at $t = 6000$ from all three models are compared (the red dotted line indicates KS, dashed blue indicates fully nonlinear coordinate-free, and solid black indicates weakly nonlinear coordinate-free). (Colour available online.)

smoothly decays. These solutions are depicted in Figure 6 and have initial data

$$y(x, 0) = 0.1 \cos\left(\frac{2\pi}{50}x\right) + 0.1 \cos\left(\frac{4\pi}{50}x\right).$$

5. Conclusion

In this work, we present a numerical method for the simulation of coordinate-free models for flame fronts. A coordinate-free model can be simulated at similar expense to the weakly nonlinear KS equation but without the restrictions of small initial data. We use this solver to simulate both weakly and fully nonlinear models, comparing the solutions in a regime where they approximate one another. We also provide simulations outside this regime, where coordinate-free models allow for overturned solutions and pinch-off. The KS equation is well known to have parameter regimes that exhibit

https://doi.org/10.1017/S1446181121000079 Published online by Cambridge University Press

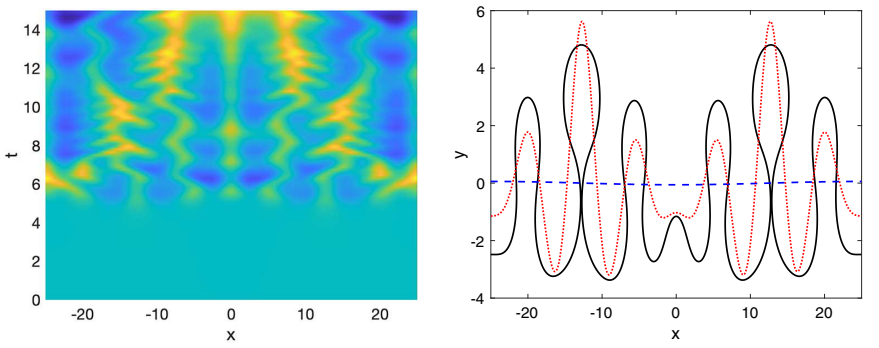

FIGURE 6. Left: a chaotic trajectory of the KS equation with $L = 50, \alpha = 9$. Right: the solutions to KS (red dotted curve), the weakly nonlinear coordinate-free model (1.2) (black solid curve) and the fully nonlinear model (1.1) (blue dashed curve) at $t = 4.75$, just before the weakly nonlinear coordinate-free solution (solid black curve) self-intersects. (Colour available online.)

travelling waves, periodic solutions and chaotic trajectories; future applications of this method include characterizing these parameter regimes for coordinate-free models. This methodology could also be applied to the higher (2D+1)-dimensional problem [8], which has not been extensively studied.

Acknowledgements

The first author acknowledges support by the Air Force Office of Scientific Research though the Computational Mathematics Program. The second author gratefully acknowledges support from the National Science Foundation through grant DMS-1907684. The authors also thank J. Douglas Wright for helpful conversations.

References

[1] B. F. Akers, D. M. Ambrose, K. Pond and J. D. Wright, "Overturned internal capillary-gravity waves", *Eur. J. Mech. B Fluids* **57** (2016) 143–151; doi:10.1016/j.euromechflu.2015.12.006.

[2] B. F. Akers, D. M. Ambrose and J. D. Wright, "Gravity perturbed crapper waves", *Proc. Roy. Soc. A Math. Phys. Eng. Sci.* **470** (2014) 20130526; doi:10.1098/rspa.2013.0526.

[3] D. M. Ambrose, F. Hadadifard and J. D. Wright, "Well-posedness and asymptotics of a coordinate-free model of flame fronts", Preprint, 2020, arXiv:2010.00737v1.

[4] U. M. Ascher, S. J. Ruuth and B. T. R. Wetton, "Implicit-explicit methods for time-dependent partial differential equations", *SIAM J. Numer. Anal.* **32** (1995) 797–823; doi:10.1137/0732037.

[5] C.-M. Brauner, M. L. Frankel, J. Hulshof, A. Lunardi and G. I. Sivashinsky, "On the κ- θ model of cellular flames: existence in the large and asymptotics", *Discrete Contin. Dyn. Syst. Ser. S* **1** (2008) 27–39; doi:10.3934/dcdss.2008.1.27.

[6] M. L. Frankel, P. V. Gordon and G. I. Sivashinsky, "On disintegration of near-limit cellular flames", *Phys. Lett. A* **310** (2003) 389–392; doi:10.1016/S0375-9601(03)00385-2.

[7] M. L. Frankel and G. I. Sivashinsky, "On the nonlinear thermal diffusive theory of curved flames", *J. Phys.* **48** (1987) 25–28; doi:10.1051/jphys:0198700480102500.

[8] M. L. Frankel and G. I. Sivashinsky, "On the equation of a curved flame front", *Phys. D* **30** (1988) 28–42; doi:10.1016/0167-2789(88)90096-6.

[9] M. Goto, K. Kuwana and S. Yazaki, "A simple and fast numerical method for solving flame/smoldering evolution equations", *JSIAM Lett.* **10** (2018) 49–52; doi:10.14495/jsiaml.10.49.

[10] T. Y. Hou, J. S. Lowengrub and M. J. Shelley, "Removing the stiffness from interfacial flows with surface tension", *J. Comput. Phys.* **114** (1994) 312–338; doi:10.1006/jcph.1994.1170.

[11] T. Y. Hou, J. S. Lowengrub and M. J. Shelley, "The long-time motion of vortex sheets with surface tension", *Phys. Fluids* **9** (1997) 1933–1954; doi:10.1063/1.869313.

[12] A. Kalogirou, E. E. Keaveny and D. T. Papageorgiou, "An in-depth numerical study of the two-dimensional Kuramoto–Sivashinsky equation", *Proc. Roy. Soc. A Math. Phys. Eng. Sci.* **471** (2015) 20140932; doi:10.1098/rspa.2014.0932.

[13] A.-K. Kassam and L. N Trefethen, "Fourth-order time-stepping for stiff PDEs", *SIAM J. Sci. Comput.* **26** (2005) 1214–1233; doi:10.1137/S1064827502410633.

[14] P. A. Milewski and E. G. Tabak, "A pseudospectral procedure for the solution of nonlinear wave equations with examples from free-surface flows", *SIAM J. Sci. Comput.* **21** (1999) 1102–1114; doi:10.1137/S1064827597321532.

[15] D. T. Papageorgiou and Y. S. Smyrlis., "The route to chaos for the Kuramoto–Sivashinsky equation", *Theor. Comput. Fluid Dyn.* **3** (1991) 15–42; doi:10.1007/BF00271514.

[16] Y. S. Smyrlis and D. T. Papageorgiou, "Predicting chaos for infinite dimensional dynamical systems: the Kuramoto–Sivashinsky equation, a case study", *Proc. Natl. Acad. Sci.* **88** (1991) 11129–11132; doi:10.1073/pnas.88.24.11129.